THE BELL SYSTEM TECHNICAL JOURNAL
Vol. 55, No. 9, November 1976
Printed in U.S.A.

Exact Theory of TE-Wave Scattering From Blazed Dielectric Gratings

By D. MARCUSE

(Manuscript received April 9, 1976)

We present an exact description of scattering of an incident plane wave with TE-polarization at an interface between two dielectric media that is deformed by a grating with triangularly shaped teeth. The theory employs an expansion in plane waves outside of the grating region and describes the field in the grating region as a double Fourier series expansion. The results of this theory are represented graphically. That blazing provides substantial discrimination of the scattering process in favor of beams scattered into one or the other of the two media is shown. The exact theory is used to check an approximation for the effective reflection plane that is useful for future applications of the theory to scattering by gratings of guided waves in thin-film waveguides.

I. INTRODUCTION

This study of dielectric sawtooth gratings with deep grooves serves several purposes. Its principal aim is to investigate a particular analytical method for describing deep gratings with the view of applying it (at a later time) to waveguide-grating couplers. However, even without the added complication of one more dielectric interface that characterizes the waveguide problem, an examination of the response of dielectric gratings with deep grooves to a plane wave, incident at an angle that would lead to total internal reflection at the corresponding smooth surface, can teach us much about the expected behavior of waveguide-grating couplers.

The literature on the electromagnetic theory of diffraction gratings is vast. However, most papers are limited to discussions of metallic gratings,[1,2] and only a few papers mention dielectric gratings with sawtooth-shaped grooves and plane waves incident at angles larger than the critical angle for total internal reflection.[3] When it comes to providing numerical information for a given particular case, each worker must write a computer program to solve the problem at hand, since no publication can cover all conceivable cases in graphical form.

Developing the computer program for the study of deep gratings was one of the aims of this work.

Our method for treating TE-wave interaction with deep dielectric sawtooth gratings is basically simple and exact. We express the field above and below the grating as a series of plane waves using the periodicity imposed by the grating. In the grating region, the field is expressed as a double Fourier series expansion whose terms are not individually solutions of the wave equation. The unknown coefficients entering the various series expansions are determined by the requirement that the field in the grating region must be a solution of the wave equation and by enforcing the proper boundary conditions along two mathematical planes just above and below the grating region. By varying the number of terms used in the series expansions, it was found that the series converge very well, and good accuracy is obtained with relatively few terms. However, the required number of terms increases with increasing depth of the sawtooth grating.

The simple grating problem described here has the advantage that only an inhomogeneous equation system needs to be solved. Since the problem does not contain unknown eigenvalues, no search for suitable eigenvalue conditions is required. The exact solution of the corresponding waveguide problem would lead to an eigenvalue equation. A very large determinant with complex coefficients would have to be forced to vanish by proper choice of the propagation constant of the leaky wave inside the guide, one of whose interfaces between core and cladding is formed by the grating. The simple grating furnishes important information about the phase shift suffered by the reflected plane waves. This information can be used to estimate the eigenvalues of the modes inside of the waveguide with a grating on one of its interfaces. This information is useful for finding approximate solutions of the waveguide grating problem without the need for solving a costly and time-consuming eigenvalue problem.

For shallow gratings, our theory is in complete agreement with perturbation theory. Some of the features of deeper gratings with groove depth on the order of the wavelength can be explained by geometrical optics coupled with simple grating conditions. The ray paths in deep gratings (groove depth larger than the wavelength) are so complicated that an explanation of maxima or minima in terms of geometrical optics fails.

The sawtooth-shaped interface deformation is a blazed grating. It has the advantage that its shape can be adjusted to enhance certain grating orders. In particular, it is possible to let a high grating order predominate over lower orders. Furthermore, the grating shape can be used to favor scattering into the air space above the grating or, cor-

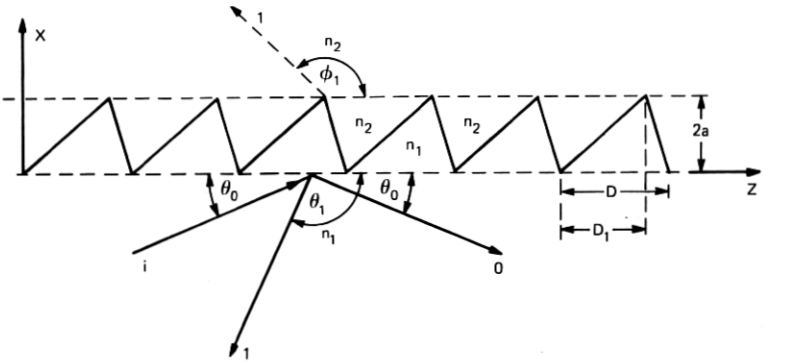

Fig. 1—Triangularly shaped dielectric grating as an interface between the two media with index n_1 and n_2. (This figure defines grating parameters and incident and scattered beams.)

respondingly, to favor scattering down into the higher dielectric region, the substrate, from which the incident wave impinged on the grating. This preferential scattering behavior is very useful for the construction of grating couplers. Additional grating responses, other than those used for the coupling beam, decrease the overall efficiency of a grating coupler. If unwanted grating lobes can be suppressed by properly shaping the grating teeth, higher coupling efficiencies are obtainable. Gratings that show strong asymmetry in favor of a certain grating order provide also high-reflection losses for the zero-order grating lobe (that would correspond to the guided mode field of a waveguide). The waveguide mode thus would decay rapidly over a few periods of the zig-zag path of the guided ray. This means that high-efficiency grating couplers based on this principle would have to be very short.

1.1 Theory of the dielectric sawtooth grating

Figure 1 shows the geometry of our sawtooth grating. A ray labeled i is incident from the medium with refractive index n_1 on the dielectric interface with the medium n_2 whose shape is a sequence of sawteeth. The specularly reflected beam is labeled 0. Also shown are two scattered beams labeled 1 which escape into the medium with index n_2 (subsequently to be called the air space) and into the medium with index n_1 (subsequently to be called the substrate). The grating period is D; D_1 is the distance along the base of each sawtooth from its beginning to the point underneath its peak. The grating amplitude is defined as $2a$.

We consider only TE-waves with the electric field component E_y and the magnetic field components[4]

$$H_x = -\frac{i}{\omega\mu_o}\frac{\partial E_y}{\partial z} \tag{1}$$

and

$$H_z = \frac{i}{\omega\mu_o}\frac{\partial E_z}{\partial x}. \tag{2}$$

(ω and μ_o are, respectively, the angular frequency of the wave and the magnetic permeability of vacuum.) The grating is infinitely extended in y direction, so that all y-derivatives vanish. The field components E_x, E_z, and H_y do not exist. The periodicity of the infinitely extended (in z direction) grating forces the electromagnetic field to be of the following form:

$$E_y = e^{-i\beta_i z}\left\{A_o^{(i)}e^{-i\sigma_o x} + \sum_{m=-\infty}^{\infty} A_m e^{i\sigma_m x}e^{i(2\pi/D)mz}\right\} \qquad \text{for } x \leqq 0, \tag{3}$$

and

$$E_y = e^{-i\beta_i z}\sum_{m=-\infty}^{\infty} C_m e^{-i\rho_m x}e^{i(2\pi/D)mz} \qquad \text{for } x \geqq 2a. \tag{4}$$

Since E_y must satisfy the wave equation

$$\frac{\partial^2 E_y}{\partial x^2} + \frac{\partial^2 E_y}{\partial y^2} + n^2k^2E_y = 0 \tag{5}$$

with

$$k = \frac{2\pi}{\lambda_o} = \omega\sqrt{\epsilon_o\mu_o} \tag{6}$$

(λ_o = free space wavelength, ϵ_o = dielectric permittivity of vacuum, $n = n_1$ or n_2 refractive index of the dielectric medium), the parameters appearing in (3) and (4) must have the form,

$$\sigma_m = \left[n_1^2k^2 - \left(\beta_i - \frac{2\pi}{D}m\right)^2\right]^{\frac{1}{2}} \tag{7}$$

and

$$\rho_m = \left[n_2^2k^2 - \left(\beta_i - \frac{2\pi}{D}m\right)^2\right]^{\frac{1}{2}}. \tag{8}$$

A_i is the amplitude of the incident wave with propagation constant

$$\beta_i = n_1k\cos\theta. \tag{9}$$

The term propagation constant is used here in the same sense as in a waveguide; it is actually the z component of the plane wave propagation vector.

Note that the superposition of plane waves (3) and (4) was chosen so that the traveling parts of the wave move away from the grating with the exception of the incident wave of amplitude $A_o^{(i)}$ [the time dependence is understood to be $\exp(i\omega t)$]. It is clear that only a small

number of waves in the field expansions actually propagate in x direction, because almost all terms of the form (7) and (8) are imaginary. The signs of the imaginary quantities must be chosen, so that the evanescent fields decay in the direction away from the grating,

$$\sigma_m = -i|\sigma_m|, \qquad \rho_m = -i|\rho_m|. \tag{10}$$

Every term in the expansion (3) and (4) is a solution of the wave equation, but a similar expansion cannot be written down for the field in the grating region $0 \leqq x \leqq 2a$. Instead, we simply use a doubly infinite Fourier series.

$$E_y = e^{-i\beta_i z} \sum_{n,m=-\infty}^{\infty} B_{nm} e^{i(\pi/b)nx} e^{i(2\pi/D)mz} \qquad 0 \leqq x \leqq 2a. \tag{11}$$

Except for the phase factor $\exp(-i\beta_i z)$, the field solution is periodic in z with period D. This periodicity is a very important feature of the field solution and is imposed by the periodicity of the grating. The function (11) is also periodic in x direction with period length $2b$. This periodicity is quite arbitrary. It would appear natural to let $b = a$. However, this choice of b would force the field to have exactly the same values at $x = 0$ and $x = 2a$, which is physically unreasonable. For this reason, we must allow b to be arbitrary, but use $b > a$. As a practical matter $b = \sqrt{2}a$ has been used for the numerical calculations in the hope that this choice would facilitate the convergence of the series. Clearly, b should not be made too large and, of course, it must not be smaller than a.

It now remains to determine the expansion coefficients A_m, C_m, and B_{nm}. This is accomplished by substituting (11) into the wave equation (5), multiplying the resulting equation with $\exp(-i\pi n\, x/b)$ $\exp(-i2\pi m\, z/D)$ and integrating over z from 0 to D and over x from 0 to $2a$. Continuity of the fields at the planes $x = 0$ and $x = 2a$ requires us to force E_y and its x-derivative to be continuous at these planes. After elimination of A_m and C_m from the equation systems, we are left with the following three infinite simultaneous equations:

$$\sum_{n=-\infty}^{\infty} \left(\rho_m + \frac{\pi}{b} n\right) B_{nm} e^{i(2\pi/b)na} = 0. \tag{12}$$

$$\sum_{n=-\infty}^{\infty} \left(\sigma_m - \frac{\pi}{b} n\right) B_{nm} = 2\sigma_o A_o^{(i)} \delta_{mo}. \tag{13}$$

$$\sum_{n',m'=-\infty}^{\infty} \left\{ N_{n'-n,m'-m} - \left[\left(\frac{\pi n'}{b}\right)^2 + \beta_{m'}^2\right] M_{n,n'} \delta_{m,m'} \right\} B_{n'm'} = 0. \tag{14}$$

$\delta_{mm'}$ is Kronecker's delta symbol. In (12) and (13) m is allowed to be

any integer, and, similarly, n and m are allowed to be any integer in (14). The first two equations stem from the boundary conditions, while (14) expresses the requirement that the field expansion (11) satisfy the wave equation (5). The three sets of infinite equations (12) through (14) are used to express B_{nm} in terms of $A_0^{(i)}$. The coefficients $N_{n'-n,m'-m}$ and $M_{n,n'}$ are listed in the Appendix; β_m is defined as

$$\beta_m = \beta_i - \frac{2\pi}{D} m. \tag{15}$$

The amplitude coefficients A_m and C_m are obtained in terms of B_{nm} as follows:

$$A_m = \left(\sum_{n=-\infty}^{\infty} B_{nm} \right) - A_0^{(i)} \delta_{m0}. \tag{16}$$

$$C_m = \sum_{n=-\infty}^{\infty} B_{nm} e^{i[\rho_m + (\pi/b)n]2a}. \tag{17}$$

The power of the incident wave flowing through an element of unit area parallel to the x direction is given as

$$P_i = \frac{\sigma_0}{2\omega\mu_0} |A_0^{(i)}|^2. \tag{18}$$

It is convenient to express the power carried away by the scattered beams in terms of the power of the incident beam. For the grating orders carrying power into the air space, we obtain the relative power from

$$\frac{\Delta P_{ma}}{P_i} = \frac{\rho_m}{\sigma_0} \frac{|C_m|^2}{|A_0^{(i)}|^2}. \tag{19}$$

Similarly, we obtain the relative power carried into the substrate,

$$\frac{\Delta P_{ms}}{P_i} = \frac{\sigma_m}{\sigma_0} \frac{|A_m|^2}{|A_0^{(i)}|^2}. \tag{20}$$

Let us close this section with a few remarks about the numerical solution of the equation systems (12) through (14). As mentioned above, the terms in the series expansions (3) and (4) represent traveling as well as evanescent waves. It is clear that all terms corresponding to traveling waves must be included in the truncated series expansions used for approximate numerical solutions of the problem. According to (7), propagating grating orders are associated with m values in the interval

$$\left[\frac{D}{2\pi} (\beta_i - n_1 k) \right]_{\text{int}} < m < \left[\frac{D}{2\pi} (n_i k + \beta_i) \right]_{\text{int}}. \tag{21}$$

The label "int" is a reminder that the integer, whose absolute value is

just smaller than the value inside of the bracket, must be taken. Those terms in the series expansion (3) whose m-values lie outside the interval (21) belong to evanescent waves that do not carry away power. As a practical matter, we found that sufficient accuracy is obtained if just one—or at most a few—evanescent waves on each side of the interval (21) are included in the series expansions. The terms in the expansion (11) cannot be interpreted as traveling or evanescent waves. The sum over m is, of course, intimately related to the m-summations in (3) and (4), and an equal number of terms must be taken in all m-summations. We found that the n-summation in (11) converges more slowly, so that usually more terms are required in this series. In all numerical calculations whose discussions follow, we never used more than 11 terms in the n-summation, and often as few as 7 terms proved to be sufficient, if the grating amplitude remained below $2a/\lambda_o = 0.5$. The total number of unknowns B_{nm} in the equation system (12) through (14) is, of course, the product of the number of terms in both series expansions, n and m. For large values of $2a$, for example for $2a/\lambda_o = 2$, we used 66 unknowns B_{nm}, and for $2a/\lambda_o < 0.5$, 36 unknowns seemed to be sufficient.

The fact that the equations stemming from the boundary conditions (12) and (13) must be included in the equation system to be solved prevents us from using an equal number of terms in the n', m' summations of (14) and for the "free" indices n and m. Obviously, the number of m-values [the number of equations of the type (14)] that are used must be two less than the number of terms under the m-summation sign.

1.2 Geometrical optics considerations

Figure 1 shows the principal function of the diffraction grating. The incident plane wave breaks up into several components after striking the dielectric interface. The strongest wave leaving the grating region is usually the zero-order grating response that leaves in a direction corresponding to the specularly reflected beam at an ideal, smooth interface. Throughout this discussion, we assume that the incident wave strikes the interface at an angle θ_o that remains below the critical angle for total internal reflection at the unperturbed, smooth boundary. In addition to the incident and specularly reflected plane waves, a discrete number of scattered plane waves are generated. These waves emerge in directions that are defined by the condition that all scattered waves interfere constructively. The condition for such constructive interference is expressed by the relation

$$\beta_m = \beta_i - \frac{2\pi}{D} m. \tag{22}$$

The β_i and β_m are the z-components of the propagation vectors of the incident and scattered waves; m is a positive or negative integer. The angles θ_m of scattered waves in medium 1 are obtained from (9) and (22) as follows,

$$\theta_m = \arccos\left(\frac{\beta_m}{n_1 k}\right), \tag{23}$$

and the corresponding scattering angles in medium 2 are

$$\phi_m = \arccos\left(\frac{\beta_m}{n_2 k}\right). \tag{24}$$

The integer m defines the grating orders of the scattered beams. The direction of the specularly scattered plane-wave is obtained by using $m = 0$, and $m = +1$ gives the first grating orders, etc.

The intensities of the scattered beams decrease with increasing grating order, if the grating amplitude $2a$ is much smaller than the wavelength. However, for deep gratings whose amplitude is comparable to, or larger than, the wavelength, higher grating orders may well predominate over lower grating orders. In particular, it is possible to predict maxima of scattered waves based on geometric optics considerations. Such maxima occur when the direction of a grating lobe defined by (23) or (24) coincides with the condition of specular reflection of the incident beam on one of the facets of the grating teeth.

Consider the situation shown in Fig. 2. Geometrical optics allow us to calculate the angle θ_m of the reflected wave as

$$\theta_m = 2\alpha_2 + \theta_o. \tag{25}$$

If θ_m simultaneously satisfies (23), a strong grating response may be

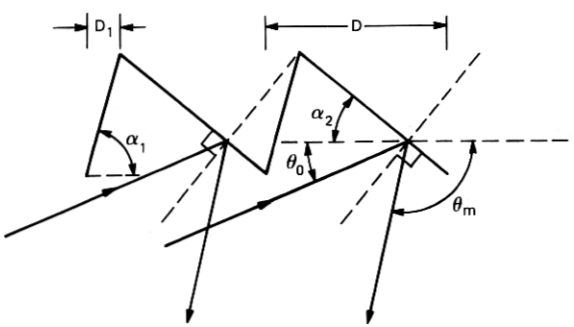

Fig. 2—Specular reflection from grating faces can be used to explain maxima of the grating lobes.

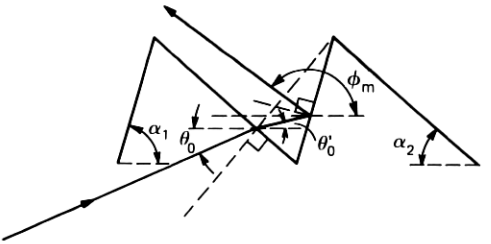

Fig. 3—Grating lobes in air can be enhanced by specular reflection from the grating teeth as shown.

expected. From (23) and (25), we find the following condition for α_2,

$$\alpha_2 = \frac{1}{2}\left[\arccos\left(\frac{\beta_i - \frac{2\pi}{D}m}{n_1 k}\right) - \arccos\left(\frac{\beta_i}{n_1 k}\right)\right]. \tag{26}$$

The grating angle α_2 is defined in terms of the other grating parameters as:

$$\alpha_2 = \arctan\left(\frac{2a}{D - D_1}\right). \tag{27}$$

Maxima for grating responses into the air space can occur in many different ways. One possibility is depicted in Fig. 3. The geometric optics condition for θ_m is computed in several steps. The refracted angle θ_o' follows from Snell's law,

$$\theta_o' = \arccos\left(\frac{n_1}{n_2}\cos(\alpha_2 + \theta_o)\right) - \alpha_2, \tag{28}$$

and the angle of the mth grating response in air follows from

$$\phi_m = 2\alpha_1 - \theta_o' = 2\arctan\left(\frac{2a}{D_1}\right) - \theta_o'. \tag{29}$$

The conditions that must be satisfied by the grating parameters to achieve equality of (24) and (29) can be found by an iterative calculation.

Geometric optics conditions leading to maxima of the grating response in air can be complicated in many ways. For example, the ray escaping into the air space shown in Fig. 3 may be intercepted by the grating tooth through which it just passed and may suffer further refraction. Another possibility is depicted in Fig. 4. The fact that many geometric optics conditions exist that may enhance the grating response in air makes it difficult to account for the maxima of the air lobes of deep gratings.

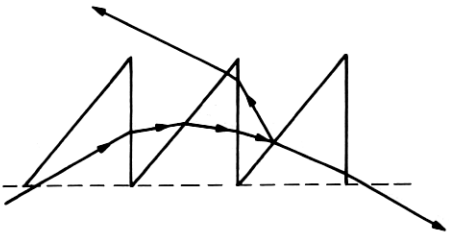

Fig. 4—The incident ray is bent back into the waveguide by successive refraction at the grating teeth. Scattering takes place at every tooth and may be enhanced if the specular reflection condition is satisfied.

Figure 4 not only shows how a ray may escape through the grating following a complicated path, but it also indicates that the unscattered portion of the ray is diffracted back into medium 1 following a path that takes it inside of the grating. This geometric optics picture suggests that the effective penetration depth of the reflected light field can be estimated by geometric optics methods. For this purpose, we assume that the grating acts on the refracted ray as a graded-index medium with an index distribution

$$\bar{n}^2(x) = \frac{2a - x}{2a} n_1^2 + \frac{x}{2a} n_2^2. \tag{30}$$

We can now use the WKB method[5] to determine the phase of the wave that penetrates into the grating region. It is well-known that the wave penetrates into the graded-index medium until it reaches the turning point of ray optics at $x = t$. The phase of the reflected wave taken at the reference plane $x = 0$ is given by[5]

$$\phi = 2 \int_o^t \sqrt{[\bar{n}(x)k]^2 - \beta_i^2}\, dx - \frac{\pi}{2} = \frac{8a\sigma_o^3}{3(n_1^2 - n_2^2)k^2} - \frac{\pi}{2}. \tag{31}$$

We define an effective reference plane by assuming that the medium with index n_1 reaches into the grating region to a depth $x = d_{app}$. The phase of a wave reflected at this reference plane (that is assumed to consist of the index discontinuity from n_1 to n_2) is

$$\phi = 2\sigma_o d_{app} - 2 \arctan \frac{\gamma}{\sigma_o} \tag{32}$$

with

$$\gamma = (\beta_i^2 - n_2^2 k^2)^{\frac{1}{2}}. \tag{33}$$

The first term in (32) accounts for the phase shift caused by the round trip from $x = 0$ to $x = d_{app}$, and the second term is the additional phase shift on reflection from the index discontinuity.[6] By equating (31) to (32), we obtain the following expression for the depth of the

effective reference surface inside of the grating:

$$d_{app} = \frac{4a\sigma_o^2}{3(n_1^2 - n_2^2)k^2} - \frac{1}{\sigma_o}\left(\frac{\pi}{4} - \arctan\frac{\gamma}{\sigma_o}\right). \tag{34}$$

If the tangent of the phase angle ψ of the reflected wave is known, for example, from the numerical solution of the grating problem, the effective reference plane can be calculated from the expression

$$d_e = \frac{2\arctan\dfrac{\gamma}{\sigma_o} - \psi \pm p\pi}{2\sigma_o}. \tag{35}$$

Note that the approximation (34) holds only for gratings that are sufficiently thick so that the turning point of the rays is located deep enough inside the grating, so that the evanescent field beyond the turning point has decayed to insignificant values by the time it reaches the top of the grating. Furthermore, (34) is certain to represent the effective reflection plane better as the grating period is short. Numerical comparisons of the two expressions (34) and (35) will be presented in the next section.

1.3 Examples and numerical evaluation

The boundary between the two media with index n_1 and n_2 is described by the function

$$f(z) = \begin{cases} \dfrac{2a}{D_1} z & 0 \leqq z \leqq D_1, \\ \dfrac{2a}{D - D_1}(D - z) & D_1 \leqq z \leqq D, \end{cases} \tag{36}$$

which is periodic in z with period D. Its Fourier coefficients are:

$$c_m = \frac{aD^2 e^{-i\pi m(D_1/D)}}{i\pi^2 m^2 D_1(D - D_1)} \sin\left(\pi m \frac{D_1}{D}\right). \tag{37}$$

This Fourier coefficient is important, because for the first order of perturbation theory[4,7] the grating responses are proportional to $|c_m|^2$.

In the remainder of this section we present the results of numerical evaluations of our theory in graphical form. Figure 5a shows the relative power that is scattered into the air space above the grating. The incident plane wave always arrives at an angle that is small enough (measured with respect to the plane interface) to ensure total internal reflection at the smooth interface between the two media. In Figs. 5 through 9, we use $\beta_i\lambda_o = 8.5$. The grating period was chosen as $D = 1.3\lambda_o$ resulting in three grating lobes labeled $m = 1$, 2, and 3.

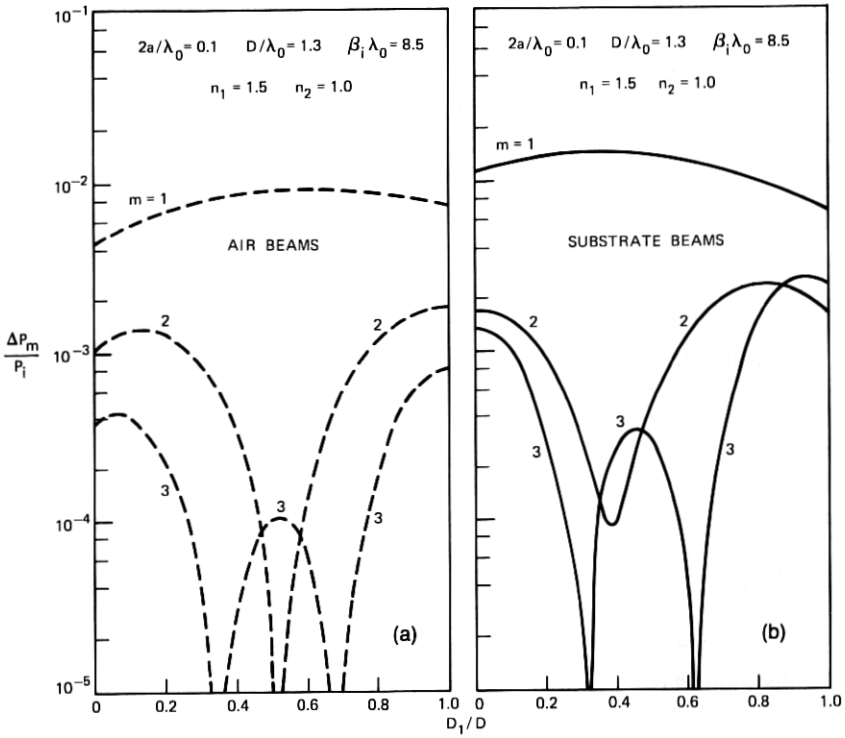

Fig. 5—Relative scattered power for the three grating lobes for $D/\lambda_o = 1.3$, $\beta_i\lambda_o = 8.5$, and $n_1 = 1.5$, $n_2 = 1.0$, and for a grating amplitude of $2a = 0.1\lambda_o$. (a) Shows the grating responses in air as functions of the grating shape factor D_1/D. (b) Shows the grating lobes in the substrate (index n_1).

The refractive index of the medium below the grating (called the substrate) is $n_1 = 1.5$, and the medium above the grating is assumed to be vacuum (or air) with $n_2 = 1.0$. The grating amplitude in Fig. 5a and b is $2a = 0.1\lambda_o$. This grating amplitude is already too large for perturbation theory to be accurate, but the zeros (or minima) and maxima of the grating responses can still be identified with the help of (37). Consider, for example, the second-order grating lobe with $m = 2$. First-order perturbation theory predicts that it has zero power at $D_1/D = 0.5$. Figure 5a for the grating responses in air shows that the zero of the second-order grating lobe is indeed very close to this value. The corresponding minimum (the power does not actually go to zero) for the substrate beam with $m = 2$ is, according to Fig. 5b, located at $D_1/D = 0.4$. Its position is shifted from the value that perturbation theory would predict, but the reason for the occurence of this minimum is still clearly discernible. The zeros for the third-order grating lobe, $m = 3$, would be located at $D_1/D = \frac{1}{3}$ and

$D_1/D = \frac{2}{3}$, if perturbation theory would apply. Correspondingly, Fig. 5a and b show that the zeros of the third-order grating responses are indeed close to these values.

Another interesting relationship results if we compare the power carried by the beams at $D_1/D = 1$. According to perturbation theory, we should find that the power ratio between the grating lobes $m = 1$ and $m = 2$ is 4, while the ratio between the lobes with $m = 1$ and $m = 3$ should be 9. According to Fig. 5a these power ratios are 4 and 8.8, respectively. The substrate beams shown in Fig. 5b give ratios of 3.8 and 1.8, respectively. The third-order grating response in the substrate is thus already considerably larger than perturbation theory would predict.

Figure 6a and b prove that all resemblance to perturbation theory is lost, if we increase the grating amplitude to $2a = 0.5\lambda_o$. According to perturbation theory, an increase of the grating amplitude by a factor of 5 should increase the scattered power by a factor of 25. No

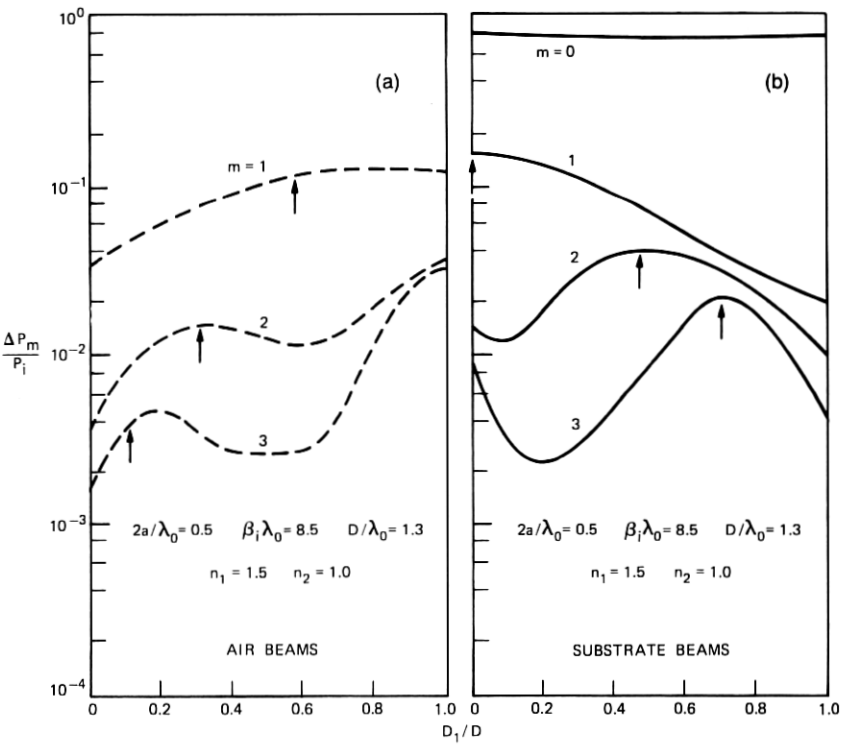

Fig. 6—Similar to Fig. 5a and b, except that the grating amplitude is $2a = 0.5\lambda_o$. (Arrows indicate the position of scattering enhancement by specular reflection from grating teeth.)

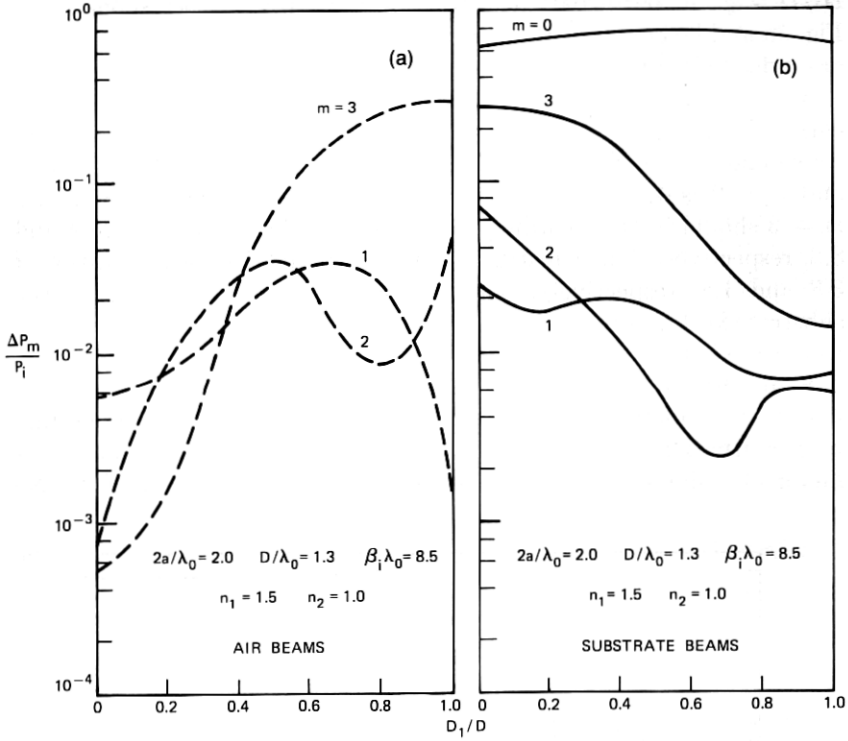

Fig. 7—Similar to Fig. 5a and b with $2a = 2.0\lambda_0$.

such increase is apparent for the first-grating order, nor is it indeed possible since the power in the scattered beams cannot exceed the input power. However, it is now possible to identify certain features of the curves by using geometrical optics. The arrows in Fig. 6a indicate the position where maxima of the grating lobes would be expected because of a coincidence of the direction of the grating lobes with specular reflection from the grating faces. The position of the arrows in Fig. 6a was computed from (24), (27), (28), and (29). Even though the agreement is not perfect, there is a strong indication that the maxima of the grating responses are indeed caused by specular reflection at the grating faces. The position of the arrows in Fig. 6b was computed from (23), (26), and (27). For the substrate lobes, the condition of specular reflection from the grating faces agrees very well with the actually observed grating maxima.

These figures show, furthermore, that very good discrimination between different grating responses can be obtained by a blazed grating. Consider a grating with $D_1/D = 1$. The first-order grating lobe in air carries 0.12 relative power while the corresponding substrate beam

carries only 0.02 relative power. The power of the higher-order grating lobes is less than one-third of the power in the first-order grating lobes. This observation has important consequences for grating couplers with blazed gratings, since loss of power to unwanted grating lobes can clearly be minimized. We shall see that even better results are obtainable with gratings that have only first-order grating lobes.

Finally, we let the grating amplitude grow to $2a = 2\lambda_o$ and show in Fig. 7a and b how the third-order grating lobe now dominates the grating response. The maxima and minima of these curves cannot easily be identified by ray tracing because of the many possible ray paths. However, the maximum at $D_1/D = 1$ of the curve with $m = 3$ in Fig. 7a seems to be caused by the specular reflection indicated in Fig. 4. The accuracy of the curves in Fig. 7a and b is not as high as that of the other figures. Whereas 42 simultaneous equations were sufficient to solve the problem with sufficient accuracy for $2a = 0.5\lambda_o$, 66 simultaneous equations were used to produce Fig. 7a and b. Computing time increases with the third power of the equation number. The accuracy of the curves in Fig. 6a and b is better than 10 percent, but the accuracy of the curves in Fig. 7a and b is poorer. However, these curves are certainly correct to order of magnitude and have the correct shapes.

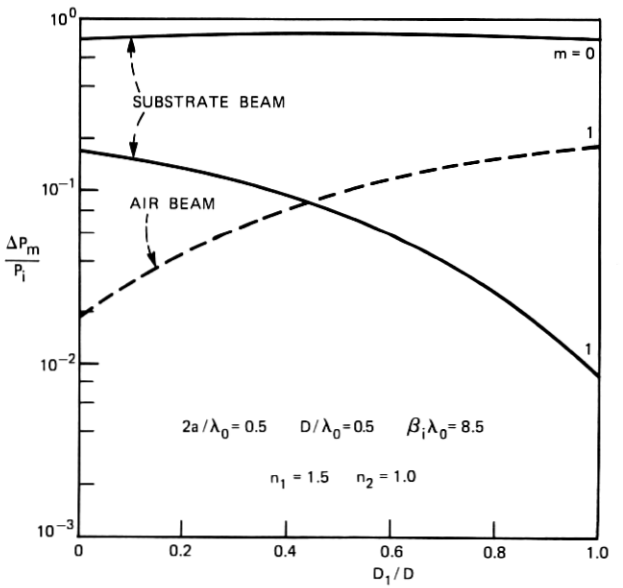

Fig. 8—Grating with only first order lobes. $D/\lambda_o = 0.5$, $\beta_i\lambda_o = 8.5$, $n_1 = 1.5$, $n_2 = 1.0$, and $2a/\lambda_o = 0.5$. The dotted line represents the relative scattered power in air; the solid lines represent the power in the substrate.

To gain insight in the beneficial effects of blazed gratings, a grating with only first-order lobes, $D/\lambda_o = 0.5$, $\beta_i\lambda_o = 8.5$, and an amplitude of $2a = 0.5\lambda_o$ was investigated. The results are plotted in Fig. 8. It is apparent that power is scattered predominantly into the substrate (solid line), if D_1/D is small and predominantly into air (dotted line) if D_1/D approaches unity. Figure 9 shows the ratio of air-to-substrate beam power for $D_1/D = 1$ as a function of the grating amplitude $2a$. Also shown in this figure is the power-reflection coefficient of the specularly reflected component; that is, the zero-order beam in the substrate. As the grating becomes deeper, the power discrimination between air and substrate beams becomes better, but the power reflection coefficient of the specular-beam component becomes lower. If we apply this situation to waveguide geometry, the incident plane wave and the reflected wave with $m = 0$ would both correspond to the guided

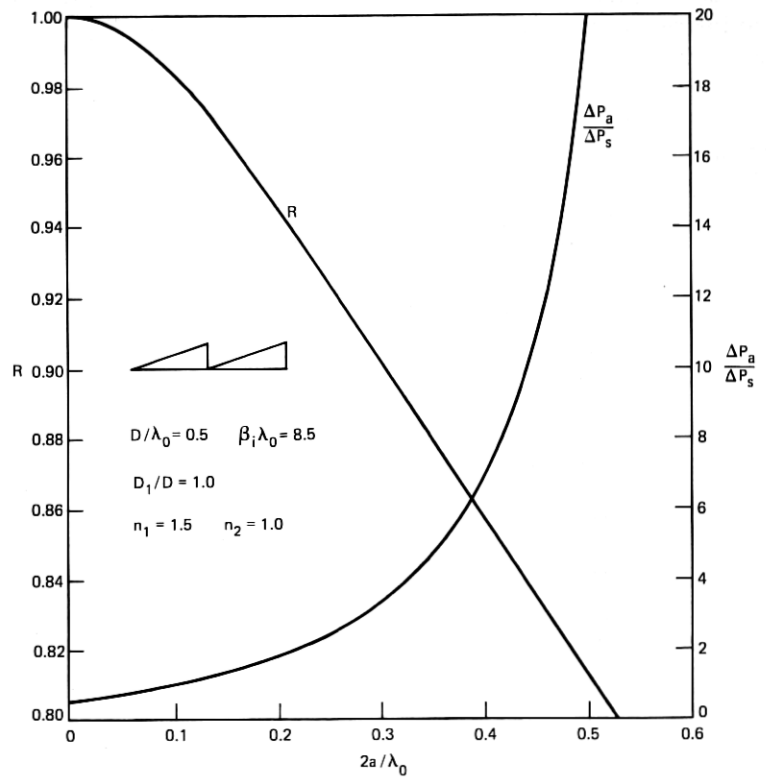

Fig. 9—Ratio of the powers $\Delta P_a/\Delta P_s$ that are scattered into air and substrate and also the power reflection coefficient R of the zero-order beam in the substrate as functions of the normalized grating depth $2a/\lambda_o$. It is $D/\lambda_o = 0.5$, $\beta_i\lambda_o = 8.5$, $D_1/D = 1.0$, $n_1 = 1.5$, and $n_2 = 1.0$.

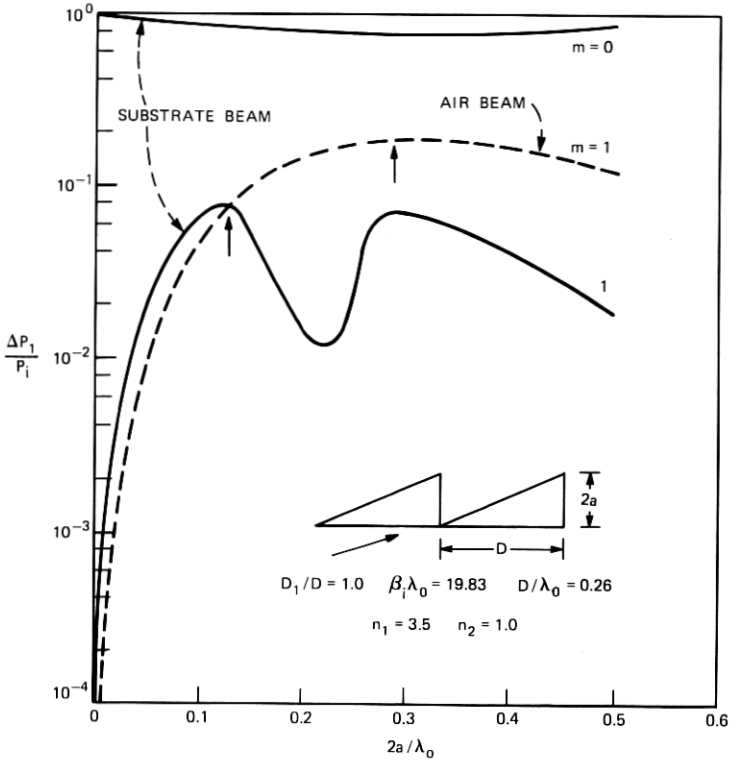

Fig. 10—Normalized scattered power into air (dotted line) and substrate (solid lines) for a grating with $n_1 = 3.5$, $n_2 = 1.0$, $D/\lambda_o = 0.26$, $D_1/D = 1.0$, and $\beta_i\lambda_o = 19.83$. The arrows indicate the position of points where specular reflection from the grating teeth coincides with the grating condition.

mode. The power loss on reflection expresses the mode attenuation per "bounce." A grating with good power discrimination between air and substrate beams suffers very high scattering losses.

Figures 10 and 11 complete our investigation of the scattering properties of blazed gratings with large-grating amplitudes. These figures apply to a substrate with high-refractive index, $n_1 = 3.5$. The gratings have $D_1/D = 1$ in Fig. 10 and $D_1/D = 0$ in Fig. 11. In both figures we used $D/\lambda_o = 0.26$ and $\beta_i\lambda_o = 19.83$. These figures show the scattered power as functions of the grating amplitude. It is obvious that the scattering levels off with increasing grating amplitude, so that it does not help to increase the grating depth beyond a certain point. However, the discrimination between air and substrate beams is affected by the grating depth. The arrows indicate points where specular reflection from the grating faces should enhance the scattered power. Except for obvious interference effects by some other ray path, it seems

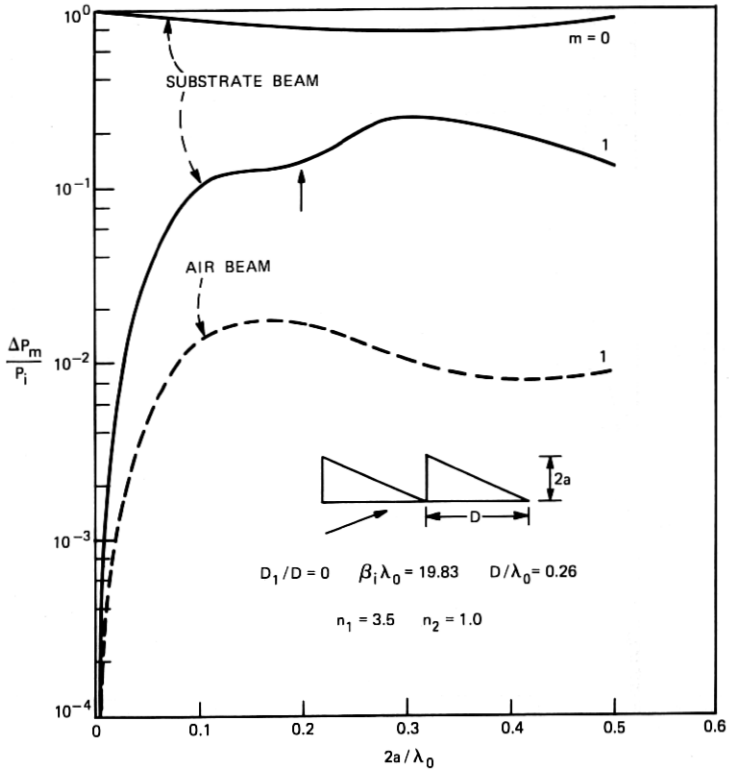

Fig. 11—Similar to Fig. 10 with $D_1/D = 0$.

that the maxima tend to be located where geometrical optics would predict.

We have extracted information about the effective reflection plane of the incident and specularly reflected plane waves. The theory of the effective reflection plane was presented in eqs. (34) and (35). Figure 12 shows the position d (normalized with respect to λ_o) of the effective reflection plane measured from the lower edge of the grating at $x = 0$. We assume that the phase of the zero-order beam in the substrate can be accounted for by reflection from an effective plane interface of the two media with index n_1 and n_2 located at $x = d$. The solid lines in Figs. 12 and 13 are obtained from our exact theory. The dotted curves represent the results of applying the WKB approximation to a continuous refractive index distribution as explained in connection with eq. (34). Figure 12 applies to a long grating period of $D/\lambda_o = 1.3$ and $n_1 = 1.5$, while Fig. 13 was drawn for $D/\lambda_o = 0.26$ and $n_1 = 3.5$. For large grating amplitudes the agreement with the approximate theory is apparently better for shorter grating periods. It might be expected

that the approximation would become very good for $D/\lambda \to 0$. Our use of the WKB approximation becomes inapplicable to $2a \to 0$. In this limit the effective reflection plane is better approximated by $d = a$. However, it is clear that the WKB approximation provides a useful estimate of the position of the effective reflection plane for deep gratings. This information is very important for an application of our theory to an approximate description of scattering by gratings on dielectric film waveguides.

The final figure, Fig. 14, shows a comparison between first-order perturbation theory and the exact grating theory. This figure represents the relative scattered powers in the first-order grating lobe (the only lobe that propagates in this case) as a function of the grating amplitude $2a$ for $D/\lambda_o = 0.5$, $\beta_i\lambda_o = 8.5$, $n_1 = 1.5$, and $n_2 = 1.0$. It is interesting to observe that the air beam is actually stronger than first-order perturbation theory would predict, while the substrate beam is considerably weaker. It is furthermore of interest that the relative strength of air to substrate-scattered power is predicted in reverse order by perturbation theory for large grating amplitudes. Whereas perturbation theory predicts that more power is scattered into the substrate than into air, the exact theory predicts just the opposite. At

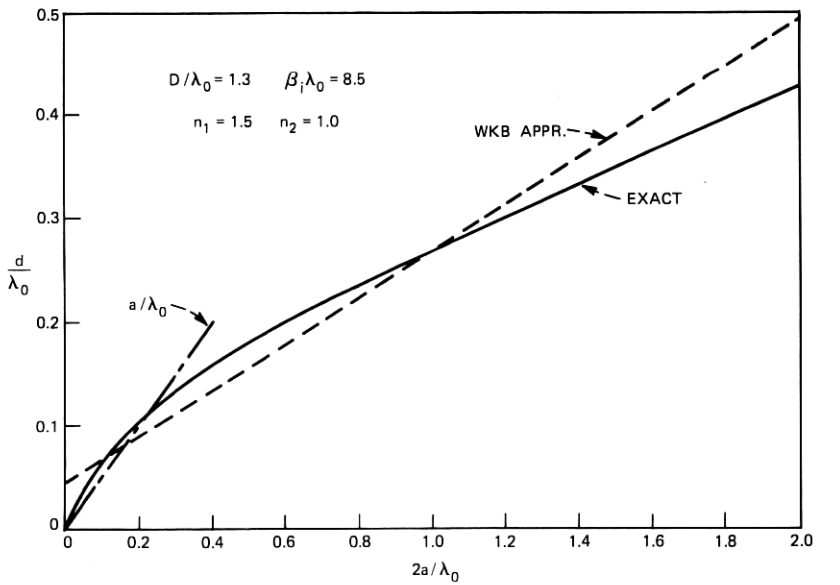

Fig. 12—Position d of the effective reflection plane as a function of grating amplitude $2a$ for $D/\lambda_o = 1.3$, $\beta_i\lambda_o = 8.5$, $n_1 = 1.5$, and $n_2 = 1.0$. The effective reflection plane is practically independent of D_1. The solid line is obtained from the exact theory while the dotted line was computed from the WKB approximation.

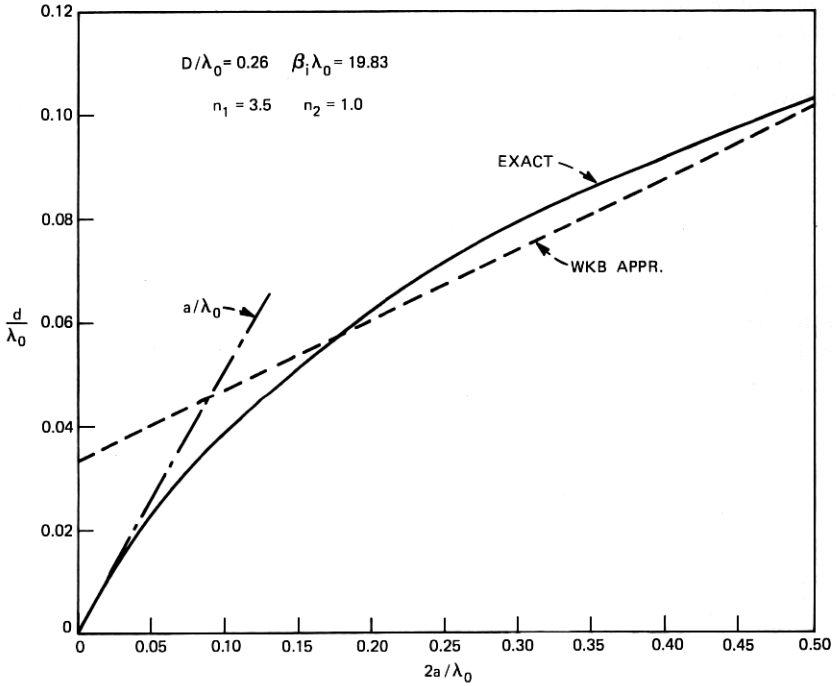

Fig. 13—Similar to Fig. 12 with $D/\lambda_o = 0.26$, $\beta_i\lambda_o = 19.83$, $n_1 = 3.5$, and $n_2 = 1.0$.

this point our theory is at variance with claims made by Tamir[3] whose results are in qualitative agreement with perturbation theory but disagree with our theory.

The arrow in Fig. 14 indicates the point at which the specular reflection condition from the faces of the grating teeth is satisfied for the substrate beam as shown in Fig. 2. This point is in good agreement with the maximum predicted by the exact theory. Perfect agreement cannot be expected for such small grating amplitudes and short grating periods, because geometrical optics cannot be expected to hold under these conditions.

Figure 14 shows that for this type of grating first-order perturbation theory is reasonably accurate for grating amplitudes below $2a = 0.05\lambda_o$.

II. CONCLUSION

We have found that our exact treatment of deep dielectric gratings with triangularly shaped teeth provides a satisfactory method for computing the scattering problem. Our theory has only been applied to incident plane waves of TE polarization. The field outside of the grating region was expanded in a series of plane waves, while the field

in the grating region was expressed as a double Fourier series expansion. Numerical evaluation of this scattering theory requires a modest computational effort. The required number of simultaneous equations that must be solved increases with increasing grating amplitude. The computer time increases with the third power of the number of equations used. For gratings with an amplitude of $2a/\lambda_o = 0.1$, 28 simultaneous equations were used, 42 equations were necessary for $2a/\lambda = 0.5$, and 66 equations were used for $2a/\lambda_o = 2.0$; however, somewhat greater accuracy seems desirable for accurate results in this latter case.

We found that blazed dielectric gratings are able to provide good discrimination of one grating lobe at the expense of other grating responses. The position of maxima and minima of the grating lobes as functions of the grating shape can be accounted for by perturbation theory for small grating amplitudes and by geometrical optics for larger grating amplitudes. However, multiple ray paths make the geometrical optics interpretation difficult for very deep gratings.

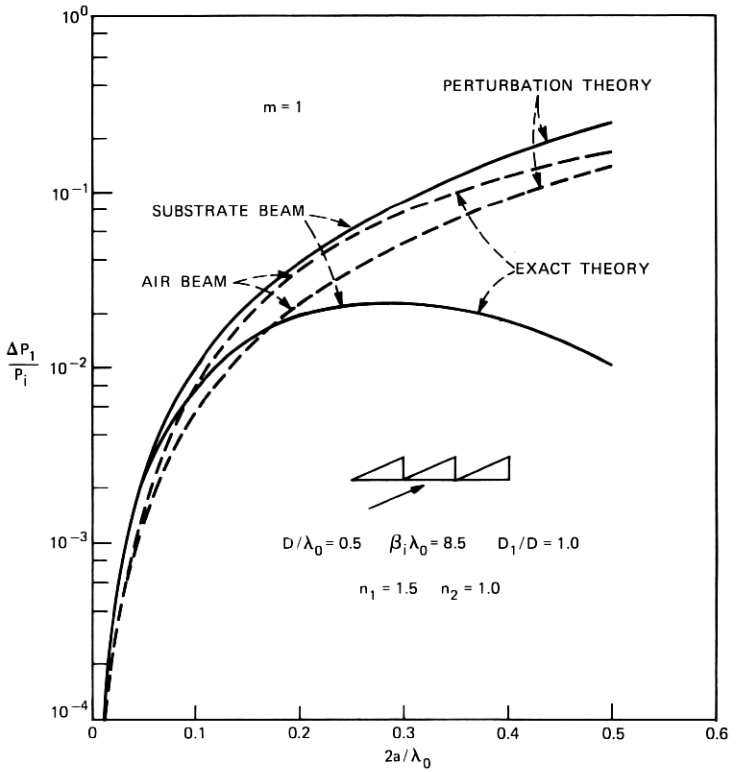

Fig. 14—Comparison with first-order perturbation theory. $D/\lambda_o = 0.5$, $D_1/D = 1$, $\beta_i\lambda_o = 8.5$, $n_1 = 1.5$, and $n_2 = 1$.

It is possible to define an effective reflection plane for the zero-order reflected grating lobe. This concept is useful for an approximate description of grating scattering of guided modes in thin dielectric films. Once the effective width of the film is known for the guided modes, scattering losses can approximately be calculated by accounting for the scattered power by means of a theory that is essentially no more complicated than the theory presented here. We have shown that the position of the effective reflection plane can be estimated by means of the WKB approximation.

III. ACKNOWLEDGMENT

I profited from fruitful discussions with W. W. Rigrod and from his considerable knowledge of the literature.

APPENDIX

We list here the coefficients that enter in the equation system (14).

$$N_{n'-n,m'-m} = \frac{(n_1^2 - n_2^2)k^2b}{2\pi^2(n' - n)} \left\{1 - \exp\left[i2\pi\left(\frac{D_1}{D}(m' - m) + \frac{a}{b}(n' - n)\right)\right]\right\} \times \left[\frac{D_1}{\frac{D_1}{D}(m' - m) + \frac{a}{b}(n' - n)} - \frac{D - D_1}{\frac{D - D_1}{D}(m' - m) - \frac{a}{b}(n' - n)}\right]$$

for $n' \neq n$ and $m' \neq m$;

$$N_{n'-n,0} = \frac{(n_1^2 - n_2^2)k^2b^2D}{2\pi^2(n' - n)^2a}\left\{1 - \exp\left[i2\pi\frac{a}{b}(n' - n)\right]\right\} + \frac{ik^2bD}{\pi(n' - n)}\left\{n_1^2 - n_2^2\exp\left[i2\pi\frac{a}{b}(n' - n)\right]\right\}$$

for $n' \neq n$;

$$N_{o,m'-m} = \frac{aD^3(n_1^2 - n_2^2)k^2}{2\pi^2(m' - m)^2D_1(D - D_1)}\left\{\exp\left[i2\pi\frac{D_1}{D}(m' - m)\right] - 1\right\}$$

for $m' \neq m$;

$$N_{0,0} = ak^2D(n_1^2 + n_2^2);$$

$$M_{n,n'} = \frac{2Dbe^{i\pi(a/b)(n'-n)}}{\pi(n' - n)}\sin\left[\pi\frac{a}{b}(n' - n)\right]$$

for $n' \neq n$;

$$M_{n,n} = 2aD.$$

REFERENCES

1. G. W. Stroke, "Diffraction Gratings," *Handbuch der Physik, 29*, S. Fluegge, ed., Springer, New York (1967), pp. 426–754.
2. R. Petit, "Electromagnetic Grating Theories: Limitations and Successes," Nouv. Rev. Optique, *6*, No. 3 (1975), pp. 129–135.
3. T. Tamir, Beam Waveguide Coupler, In Integrated Optics, T. Tamir, ed., Springer Verlag, New York (1975), pp. 83–137.
4. D. Marcuse, *Theory of Dielectric Optical Waveguides*, New York: Academic Press, 1974.
5. P. M. Morse and H. Feshbach, *Methods of Theoretical Physics, II*, New York: McGraw-Hill, 1953.
6. D. Marcuse, *Light Transmission Optics*, New York: Van Nostrand Reinhold, 1962, p. 18, Eq. (1.6–14).
7. W. W. Rigrod and D. Marcuse, "Radiation Loss Coefficients of Asymmetric Dielectric Waveguides with Shallow Sinusoidal Corrugations," unpublished work.